JOURNAL OF MATERIALS SCIENCE 29 (1994) 3643–3652

Direct observation of the fracture of CAS-Glass/SiC composites

PART I *Delamination*

H. R. SHERCLIFF
Engineering Department, Cambridge University, Trumpington St, Cambridge, CB2 1PZ, UK

G. VEKINIS
"Demokritos" National Centre for Scientific Research, Institute of Materials Science, 15310 Ag. Paraskevi Attikis, PO Box 60228, Athens, Greece

P. W. R. BEAUMONT
Engineering Department, Cambridge University, Trumpington St. Cambridge, CB2 1PZ, UK

The fracture of ceramic-matrix composites is frequently complex, involving the evolution of subcritical damage which strongly affects the final failure process, and which is very specimen dependent. In this and a companion paper, observations of fracture mechanisms are described for a calcium-alumino-silicate (CAS) glass reinforced with SiC fibres. The tests were principally undertaken dynamically *in situ* within a scanning electron microscope. This technique enables detailed characterization of the subcritical damage and of the crack interactions which occur prior to final failure. It is shown that meaningful modelling of fracture processes in these materials generally requires this level of detail in identifying the micromechanisms. This paper describes a preliminary evaluation of the unnotched tensile response of the material, followed by *in situ* observations on two common delamination geometries: four-point bending and double cantilever beam. The tensile behaviour of edge-notched specimens is described in the companion paper.

1. Introduction

In recent years considerable research effort has been applied to the processing and mechanical performance of ceramic-matrix composites (CMCs). The results presented in the literature have been examined in detail to identify those issues which could be specifically addressed using the *in situ* scanning electron microscopy (SEM) facilities at the Cambridge University Engineering Department.

A number of reviews of the mechanical properties of fibre-reinforced ceramic-matrix composites have been published [1–3]. Many studies of the strength of these materials first consider their unnotched tensile behaviour (static and fatigue), with uniaxial or bending geometries. Observation of matrix cracking has been extensive, using various methods such as acoustic emission and edge-replication microscopy [4–7], but also direct optical or SEM observation [8–11]. This work has identified the key role played by the fibre–matrix interface in promoting multiple cracking and fibre pullout. The interface has thus received considerable attention both experimentally and theoretically [12–16]. The pioneering study of multiple matrix cracking by Aveston *et al.* [17] has been extended by a number of authors to incorporate fibre, matrix and fibre–matrix interface properties [18–21].

The unnotched tensile response of SiC-fibre CMCs is therefore well established, so comparable experiments *in situ* were considered superfluous. However, a preliminary tensile test was conducted to check that the material used in this project showed similar behaviour to that reported in the literature.

The tensile response of brittle materials is frequently examined using flexural loading. In a recent review by Quinn and Morrell [22] it is emphasized that there are difficulties in conducting reproducible flexure tests with monolithic ceramics and in using the data for design purposes. The apparent ease of conducting flexure tests has led to a general acceptance of this method for ceramic long-fibre composites, but as pointed out in [22, 23] this is in many ways erroneous and potentially misleading. The stress state is much less uniform than in monolithic ceramics, due to subcritical damage initiating in the tensile half of the specimen, and shear or compressive failures commonly occur. Larsen and Stuchly [23] conclude, therefore, that at best the flexure data are comparative only, but numerically they can be misleading from the point of view of providing design data. These limitations were noted in some of the first work on SiC-reinforced ceramics (see [24], for example). Other workers have tested surface-notched specimens in four-point bending to evaluate the delamination resistance in unidirectional and cross-ply materials [25, 26]. Larsen and Stuchly's view is endorsed – the failure processes are variable, being strongly influenced by shear or compressive damage, and the results are very specimen dependent. Nevertheless, there has

0022–2461

been a major modelling effort aimed principally at predicting the R-curve response of mixed-mode-delamination cracks in flexure and tensile geometries [27–34]. Given the experimental variability of the tests, even under nominally identical conditions, the value of extensive finite-element computations is perhaps questionable. *In situ* four-point-bend tests were therefore conducted to critically evaluate the reproducibility of the damage and failure mechanisms in this popular geometry.

Delamination is predominantly a mode-II or mixed-mode phenomenon. However, the mode-I double cantilever beam (DCB) specimen offers the advantage of simplicity, with the ability to observe bridging mechanisms directly due to the significant crack opening. Fibre bridging in this geometry has been recently modelled by Spearing and Evans [35]. DCB tests were therefore conducted *in situ* to provide more detailed information on crack bridging. While the DCB geometry itself is not of any practical significance, the information gained may readily be applied to more practical mixed-mode configurations in which the crack opening is small.

Previous work in SiC-fibre-reinforced ceramics has thus guided the choice of test programme conducted *in situ* in the SEM during this project. The emphasis has been on experimental observation of the damage and failure mechanisms, rather than on the modelling. Computations relating to the common test geometries have been extensive elsewhere, so it was considered more important to question the basis of the existing models, which in some ways have run ahead of the experimental work. More extensive details of the experiments are given in [36, 37]; the dynamic *in situ* testing facilities are described in [38].

2. Experimental work, results and discussion

2.1. Material

The laminated material supplied by the USAF Materials Laboratory, Dayton, consisted of 6 and 7 ply (0/90) layups of CAS (calcium-alumino-silicate) glass reinforced by Nicalon SiC fibres. The layup method (on a rotating drum without pre-tensioning) results in a variable density of fibres, with pronounced waviness of the fibres. The average diameter of the fibres used in the USAF material was measured as 12.5 ± 1.5 μm, with a few extreme fibres outside this range. The composite matrix was an electrical-type glass (Corning Glass Works, Code 1723) whose composition is given in Table Ia. The average grain size was about 12 μm. Typical properties are given in Table Ib.

TABLE I (a) The Manufacturer's composition (wt %) of the CAS glass matrix, and (b) some properties of the glass matrix [39]

(a)

SiO_2	B_2O_3	Al_2O_3	CaO	BaO	MgO	As_2O_3
56.8	4.3	15.5	10.0	6.0	6.9	0.5

(b)

Softening point (°C)	908
Working point (°C)	1168
Coefficient of thermal expansion ($\times 10^{-6}$ K^{-1})	4.6 (0–300 °C) 5.2 (300–665 °C)
Young's modulus (GPa)	86
Density (mg m^{-3})	2640

2.2. Tensile test

A preliminary tensile test was carried out in a conventional testing machine using gauged specimens of the 7-ply material to check that the material showed comparable behaviour to other systems reported in the literature. The specimens were cut with transverse 90° plies at the surface in order to observe the formation of transverse ply cracks optically during the test. Three of the seven plies therefore lay in the tensile direction. The stress–strain response is shown in Fig. 1. The initial Young's modulus was 133 GPa up to the onset of matrix cracking, which initiated at a low strain, $\varepsilon_{mc} = 0.033\%$, with the approximately simultaneous formation of many transverse ply cracks. The nominal remote stress at this point was $\sigma_{mc} = 44$ MPa. Following the onset of matrix cracking the load-displacement response continued linearly at a lower slope corresponding to a modulus of 76 GPa. At a strain $\varepsilon_{ff} = 0.30\%$ the curve became non-linear, corresponding to the initiation of fibre fracture in the 0° plies (direct observation was not possible as these plies were subsurface). The remote stress was then $\sigma_{ff} = 246$ MPa, after which the specimen displayed extensive pseudo-plastic behaviour during fracture and pullout of the fibres. The maximum stress, $\sigma_f = 289$ MPa, was reached at a relatively large strain, $e_f = 0.65\%$. At this point the specimen failed abruptly and the stress fell to less than 10% of the maximum value. Observations of the fracture surface of the material revealed extensive fibre pullout, with mostly individual fibre failures rather than bundle failure.

2.2.1. Discussion

The initial modulus prior to matrix cracking computed by standard laminate theory is 125 GPa; this is in reasonable agreement with the measured value of 133 ± 5 GPa. It is worth noting that the material was only weakly anisotropic with calculated moduli parallel and normal to the fibres in a single uni-ply of 137 GPa and 116 GPa, respectively. The matrix cracking stress was low, around 44 MPa, corresponding to a strain of 0.033%. These are comparable to values reported for a CAS-ceramic matrix SiC material by Pryce and Smith [10]. The strain to reach fibre failure (30%) was also similar to their value. Most of the matrix cracks appeared to form near the knee in the stress–strain curve. Pryce and Smith reported continuous development of matrix cracks beyond the knee, which may also be the case here as the optical resolution was low. The tensile response of the material was therefore considered to be comparable to that of CAS-ceramic-matrix laminates reported in the literature.

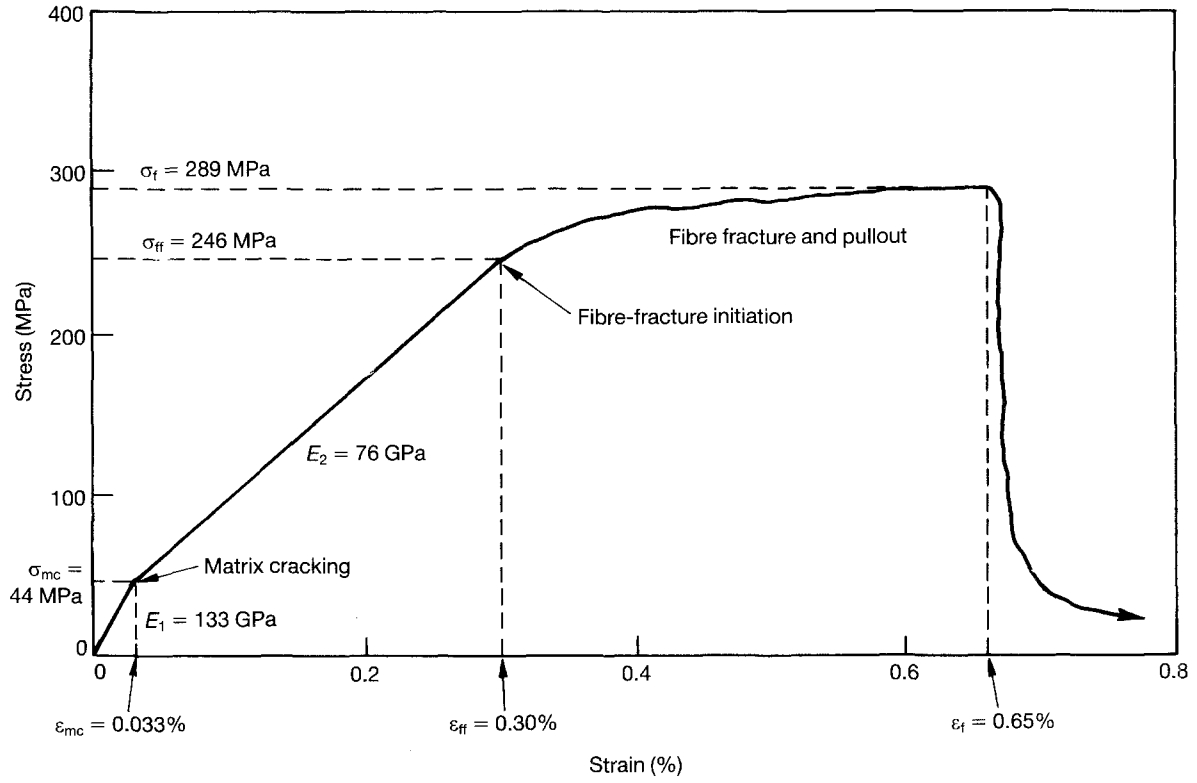

Figure 1 The stress–strain response of seven-ply (0/90) CAS-glass/SiC tested in tension with three 0° plies, gauge length = 40 mm.

2.3. Four-point bend tests

The tensile strength of brittle materials is often investigated using bending geometries. Bending also allows systematic variations in the magnitudes of the shear and direct stresses. In ceramic-composite materials such as glass–SiC the shear strength of the material is considerably lower than the tensile strength due to the weak fibre–matrix interface. The failure mechanisms in bending frequently, therefore, involve shear cracking–for example, delamination cracks parallel to the axis of the beam. Notches are often introduced to localize the failure. Most studies to date on notched or unnotched material simply calculate the maximum tensile or shear stresses by applying classical beam theory for an isotropic material. For a true understanding of failure in bending, it is necessary to examine the subcritical evolution of the damage before final failure. A comparison of different nominal strengths is meaningful if the state of damage in the test specimens is in some way self-similar at failure.

The bend tests were conducted using four-point bending, since this geometry gives a central span which is in pure bending. The material tested was the seven-ply (0/90) laminate, and the test geometry is shown in Fig. 2. Typical specimen dimensions were a beam of width 4 mm, a depth of 1.5 mm and a distance between adjacent loading points of 8 mm. In all cases the specimens had 0° plies at the surface, except for a trial experiment in a ± 45 configuration. Notches were cut through the surface ply, with the notch root at different depths in the 90° ply to see how this influenced the failure. As this geometry is commonly used, the sensitivity of the test to variations in specimen preparation requires careful assessment. The load was monitored throughout, but as it was difficult to measure the displacement *in situ* the stiffness response of the beams was not recorded. The nominal maximum tensile stress was not evaluated, since it is a potentially misleading measure of the strength in this geometry. This is because the damage in the beam is neglected, but the damage will alter the stress distribution significantly and locally affect the material modulus.

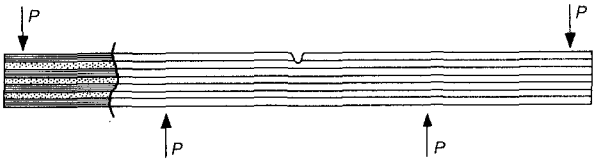

Figure 2 A schematic of the four-point-bend specimen in a seven-ply (0/90) CAS-glass/SiC.

2.3.1. The fracture behaviour of (0/90) specimens

Figs 3–5 show stages in the failure processes. The initial damage always consisted of cracks through the 90° ply, following the weak fibre–matrix interface as far as possible. The cracks ran to the next 90/0 interface, at which point they became delaminations, often running in the 0° ply a few fibres below the interface (Fig. 3a). The 90° cracks showed a small degree of *low-angle bridging* (by fibres running parallel to the notch root). This is a result of the slight misalignment of the fibres in the ply. As the load increased, the delaminations propagated in both directions and these too were bridged by low-angle fibres (Fig. 3b). It was

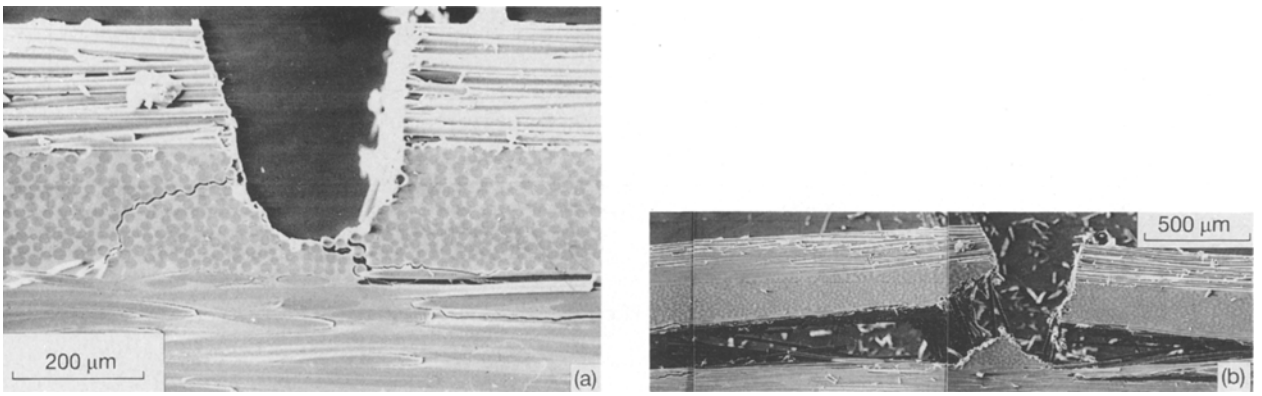

Figure 3 The development of damage from a surface notch in a four-point bend of a (0/90) CAS-glass/SiC: (a) initial cracks in 90° ply leading to interface delamination (8% of the peak load), and (b) low-angle fibre bridging of delaminations (50% of the peak load).

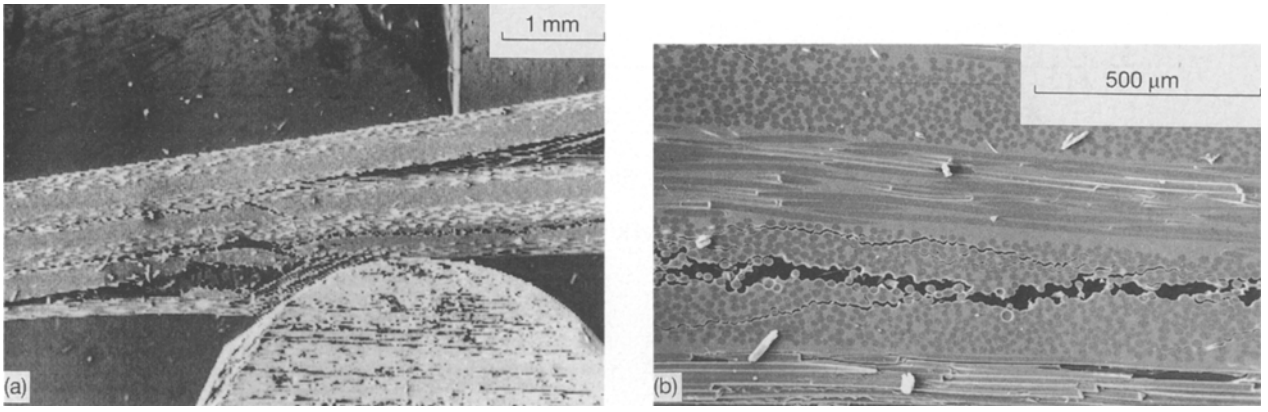

Figure 4 Shear/compression failure in a four-point-bend specimen: (a) failure of the outer span; and (b) failure of the lowest 90° ply in the central span.

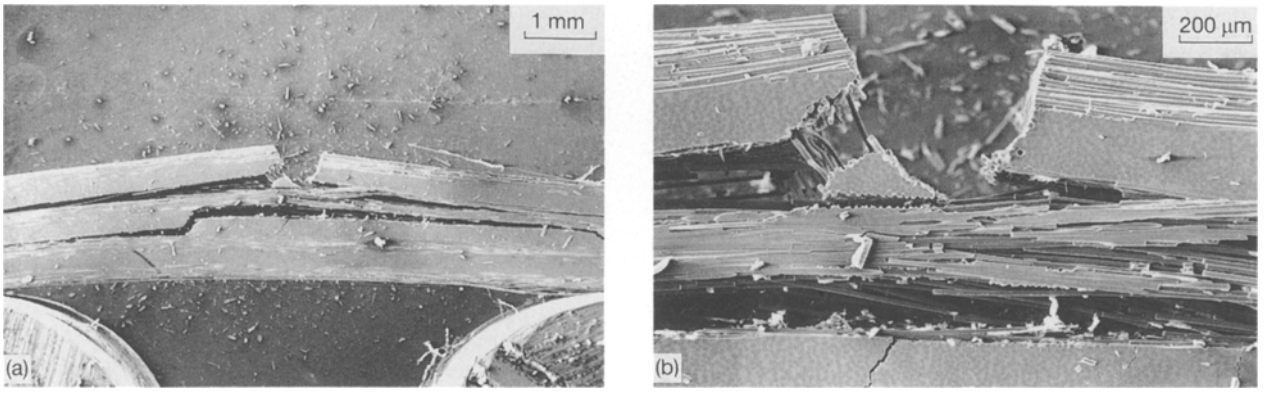

Figure 5 Tensile fracture in a four-point-bend specimen of 0° ply below the notch: (a) overall view, and (b) detail of the principal load-bearing 0° ply after failure.

apparent from specimen to specimen that the degree of bridging was very variable, due to statistical variation in fibre waviness. This led in some cases to marked asymmetry in the damage. Transverse ply cracks formed at roughly uniform intervals in the 90° ply, but these did not play any role in final failure. Once the delaminations reached the inner loading rollers, one of two mechanisms of final failure were observed: *type a* shear failure, initially in the outer spans of the specimen; or *type b* catastrophic failure of the 0° ply. Shear failure starts by propagation of the delaminations into the outer spans, followed by buckling failure of the 0° ply on the compressive face of the outer span (Fig. 4a) and by catastrophic shear failure of the lower 90° plies in the central span (Fig. 4b). Fig. 5 shows a tensile failure in which fracture of the 0° ply occurred close to the notch. The fibres are broken in a wide range of positions, leading to extensive pullout – a reflection of

the statistical (Weibull) nature of the fibre (and thus of the ply) strength. Failure of the 0° ply led to immediate propagation of delamination along the next 0/90 interface, and failure of the next 90° ply. This illustrates a benefit of dynamic testing – post-failure examination in this case would not give a true picture of the damage state, particularly of the delamination, at failure. In another case of tensile failure, the 0° ply failed several millimeters from the notch root. It is apparent, therefore, that the stress concentration of the notch is greatly diminished by the delaminations. Shear failures were characterized by a progressive collapse under falling load, whereas tensile failures were catastrophic.

In general, the deeper the notch was cut through the 90° ply the greater was the probability of tensile rather than shear failure. This is because when the notch root lies close to the next 0° ply, bridging of the delamination is established near to the notch. Propagation of the delaminations then required higher loads, due to the more extensive bridging, and load transfer into the 0° ply was more localized to the notch region. The stress in the 0° ply thus reached the tensile failure strength of the ply before the delaminations extended far into the outer span. The use of a longer span might lead to tensile failure in all cases, but the bending moment per unit width at failure would still be variable, due to statistical fluctuations in: (a) the density of the bridging fibres (and thus load transfer across the delamination), and (b) the tensile strength of the 0° plies. Note that in unidirectional material, often reported in the literature, the notch-depth effect is absent since the root of the notch always lies in a 0° ply.

2.3.2. *The fracture behaviour of (± 45) specimens*

The failure sequence in the (± 45) specimen is illustrated in Figs 6–8. The first cracks to initiate grew to one side of the notch at first, then they propagated through the next ply as a number of parallel cracks (Fig. 6a). Note again that the cracks largely follow the fibre–matrix interface. At a higher load (Fig. 6b) the first-ply interface had delaminated to the right of the notch and the second interface had failed. To the left of the notch lay a band of fibre ends which were pulled-in from the polished surface. This *fibre pull-in* is a good indication in dynamic testing that these fibres bridge a crack within the bulk of the specimen. As the crack opens, the bridging fibres debond right back to the free surface and slide away down a tube in the matrix (Fig. 7). As the load increased, the distance at which pull-in occurred to the left of the notch increased. This is consistent with a steadily increasing debond length for fibres which are all bridging cracks in the vicinity of the notch. The delamination at the second interface propagated past the notch, until parallel cracks formed through the next ply and the next interface delaminated (Fig. 8a). This process repeats, with the dominant crack path zigzagging through the specimen – it is illustrated at an advanced state of damage, with significant curvature of the specimen, in Fig. 8b. In some respects, this cracking behaviour resembles that

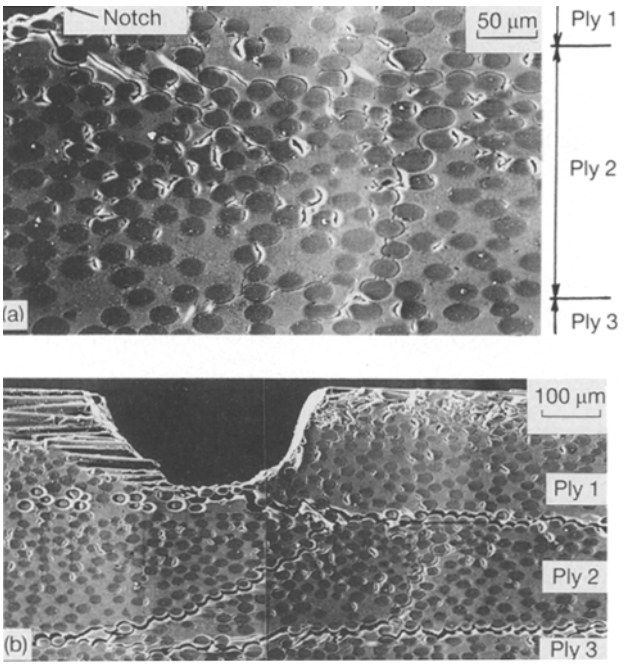

Figure 6 The development of damage from a surface notch in four-point bending of a (± 45) CAS-glass/SiC: (a) initial cracks through the first ply below the notch (50% of the peak load), (b) delamination of the first two interfaces, with bridging fibres near the notch pulled-in from the free surface (70% of the peak load).

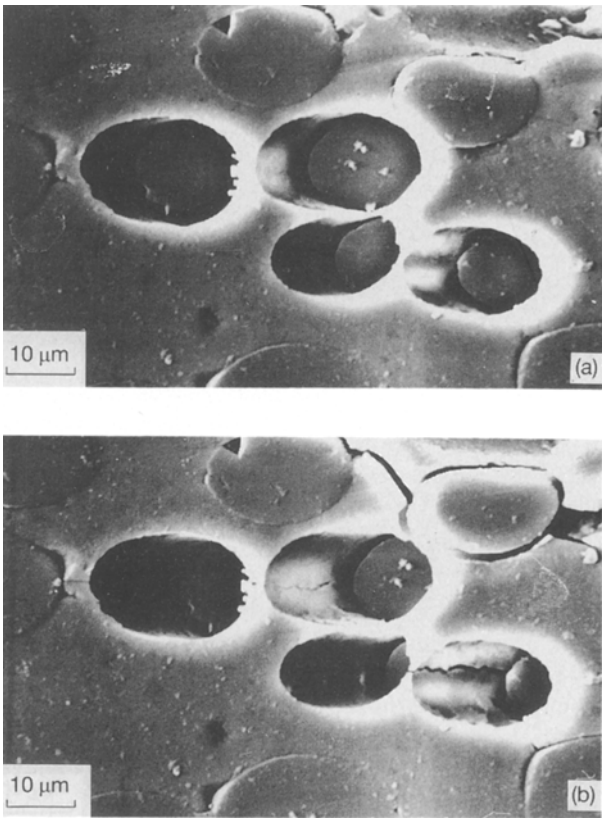

Figure 7 Detail of fibres pulled-in from the free surface near the notch at two load levels.

observed in laminated SiC [40] and also in wood [41]. Fig. 8c shows the crack paths in more detail – in the vicinity of the cracks through the plies there is extensive fibre pull-in. Blocks of material are observed to slip parallel to the fibre direction – as in the centre of

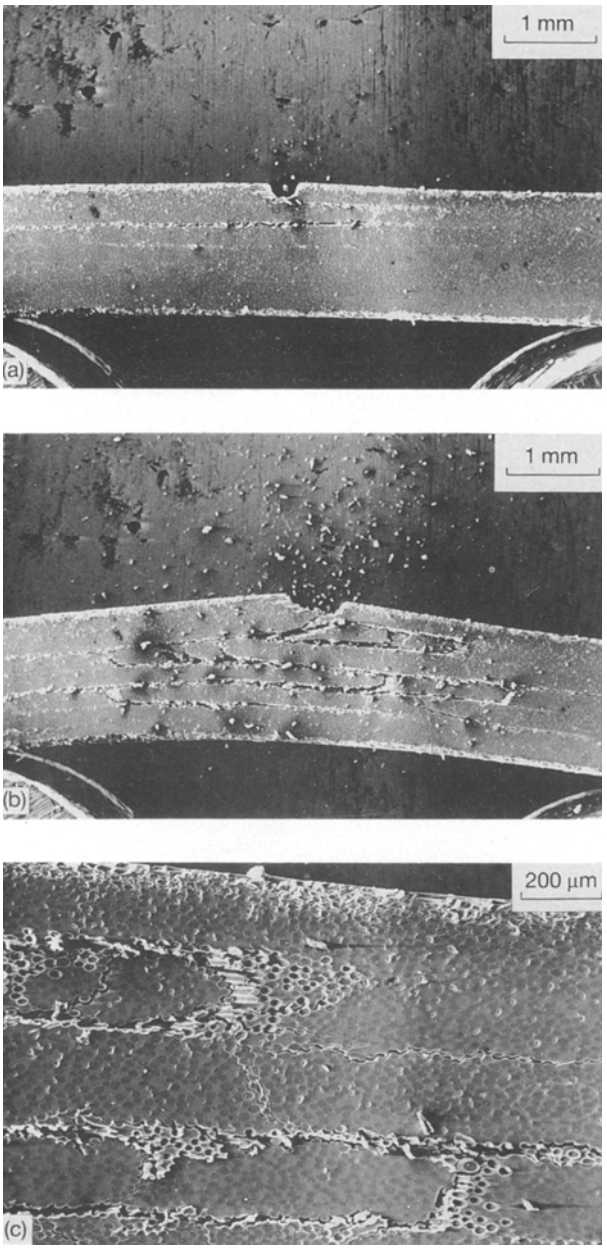

Figure 8 Progressive cracking and failure of (± 45) laminate in a four-point-bend specimen: (a) overall view, showing three failed interfaces (90% of the peak load), (b) overall view, showing extensive damage and specimen curvature near the end of the test, (c) detail of pull-in of fibres and blocks of material near cracks through the plies.

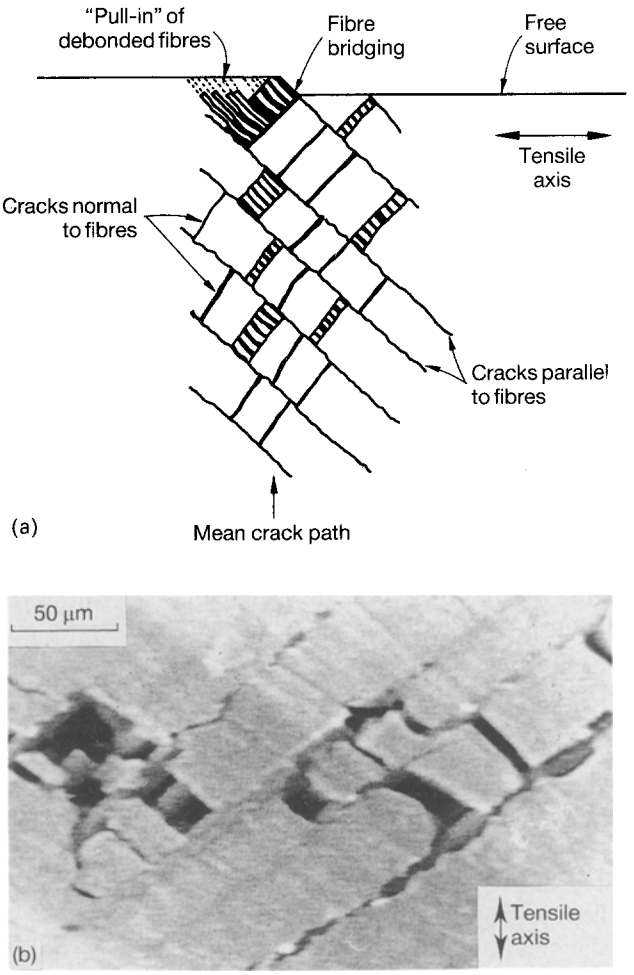

Figure 9 The bridging behaviour produced by a crack through a 45° ply: (a) a schematic view of the ply in plan view, and (b) bridging observed in a (± 45) compact tension specimen (taken from a video recording).

the second ply of Fig. 8c. The damage produced by a crack propagating through a 45° ply loaded in tension is shown schematically in Fig. 9a. The mean crack path develops by multiple cracking parallel and normal to the fibre direction. Similar observations earlier in this project [36] have been made in a (± 45) compact tension specimen; see Fig. 9b. The 45° fibre bridging thus leads to non-catastrophic failure and dissipates considerable energy. The peak bending moment (per unit width) was roughly half that obtained in the (0/90) configuration.

2.3.3. Discussion

The tests on 0/90 specimens in four-point bending suggest that the initial damage which propagates from a through-ply surface notch is broadly self-similar, but it is subject to asymmetry and lack of reproducibility. Final failure occurs by some combination of shear and compression, or by tensile failure of the most heavily loaded 0° ply. Similar tests by Bordia *et al.* [25] and Sbaizero *et al.* [26] which were not conducted *in situ* have identified the onset of tensile, compressive and shear damage coupled to kinks in the load–displacement response. As their tests use a different span-to-depth ratio, and a different inner-to-outer span ratio, the relative magnitudes of the shear and bending stresses are different. Consequently, the damage sequence observed differs from that observed in our *in situ* tests. Measurement of an *R*-curve for delamination was not made in our experiments, though the crack tips could be located very accurately. These measurements are somewhat laborious *in situ*, and the asymmetry of the damage and variability between nominally identical tests make the results of limited value in any case. Bordia *et al.* found large variations in the *R*-curves measured on a number of similar specimens.

Four-point-bend data on surface-notched specimens is thus very specimen dependent and of limited merit. It is apparent that the variability arises from: (a) the statistical variation in fibre strength and packing;

(b) variations in notch depth leading to different damage and fibre bridging; and (c) variations in ratios of specimen dimensions changing the relative importance of shear, compression and tensile stress on the damage and failure mechanisms. Studies using this geometry really need to be conducted over a wider range of loading combinations, with duplicate tests of nominally identical loading. Limits on quantities of material generally make this impossible. In our own test programme using *in situ* rigs, space restriction in the scanning electron microscope did not allow a wide variation in the four-point-bend configuration. It is clear that there is little justification for extravagant modelling of, for example, bridging of the delaminations which propagate in notched four-point-bend tests, since the damage is not experimentally reproducible.

The ± 45 specimen provided evidence of the possible benefits of incorporating 45° plies in a CMC layup. The crack path through the specimen was tortuous leading to extensive bridging and fibre pull-out (as evidenced by fibres being pulled-in from the free surface). Failure was non-catastrophic, and it dissipated considerably more energy than a conventional (0/90) laminate.

2.4. Double cantilever beam tests

The difficulty of measuring a delamination *R*-curve in the four-point-bend geometry suggests the use of a different geometry to assess the resistance of the material to delamination. The DCB method has the advantages of simplicity, with a single crack tip, and a crack path embedded in a 0° ply. The loading is however mode I, whereas practical delaminations are essentially mode II, with possibly a partial mode-I component. However, it is of value to conduct DCB tests *in situ* as a clear interpretation of mode-I fibre bridging can be obtained, due to the large crack opening, and some of this information is of value in understanding mode-II delamination, when the crack remains closed and direct observation is precluded.

2.4.2. Experimental observations of $(90/0/90)_s$

The DCB geometry used is illustrated in Fig. 10. The specimen dimensions were approximately $27 \times 10 \times 1.5\,mm^3$. The load was applied via pinned grips glued to the specimen surfaces. The $(0/90/0)_s$ layup provided a double central ply in which a 0.15 mm notch could be cut. At small loads, a crack initiated near the notch root and propagated parallel to the fibres in the double 0° ply. The crack ran down the centre of the ply, and as the crack opening increased bridging fibres could be seen, spanning the crack at a low angle (Fig. 11a). A single fibre provided both mode-I and mode-II tractions to the crack face, but as fibres bridged in both directions, overall the mode-II components approximately balanced. The bridging persisted to large crack openings with the main features being: (a) the fibres were very straight, thus they apparently carried considerable tensile forces (Fig. 11b); (b) fibres failed intermittently, and always close to the point where they emerged from the crack flanks, so that the density of the bridging fibres fell steadily with increasing crack opening behind the crack tip; and (c) the maximum angle of the bridging fibres remained below approximately 15° (that is, as the crack opened, the fibres peeled out of the matrix

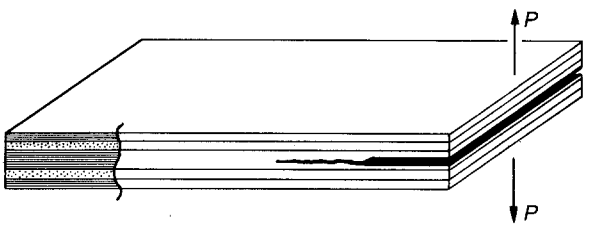

Figure 10 A schematic of the DCB specimen in $(0/90/0)_s$ CAS-glass/SiC.

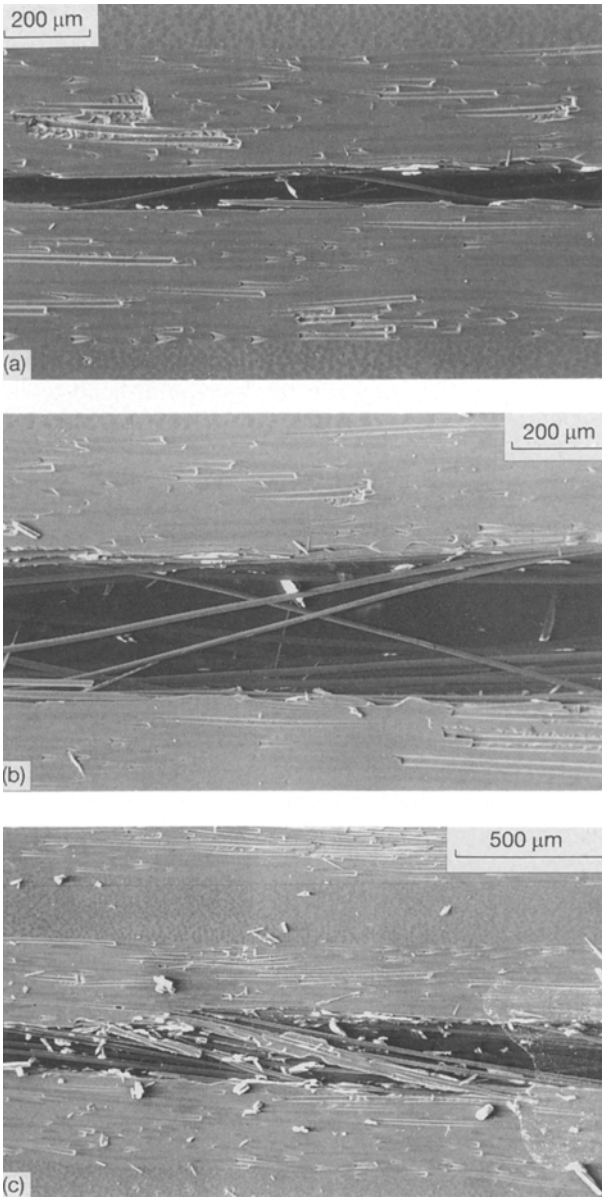

Figure 11 The development of fibre bridging in a DCB test: (a) fibres bridging at low angle (b) bridging fibres at a larger crack opening, showing the straightness of fibres, and (c) bridging by a bundle of fibres.

exposing a greater length of fibre). Occasional fibres lay at angles much greater than 15°, but these fibres were clearly less taut than the others, having a distinct curvature. Such fibres had either broken in the matrix and pulled-out, or debonded back to a free surface from which they then were able to pull-in. A second mode of bridging was occasionally observed – collections of fibres all bridging in the same direction (Fig. 11c). These bundles started as short beams with a depth of several fibres. As the crack opened the matrix broke away, leaving individual fibres acting singly, though with a net mode-II action as well as the closing mode-I behaviour.

Throughout the tests, the load was measured for a number of crack lengths. As the crack advanced stably under increasing load, it was clear that the toughness increased with crack length (that is, an *R*-curve behaviour was exhibited). Bridging fibres survived near the notch root right until the crack left the back of the specimen, so the steady-state bridging zone would be in excess of 20 mm. By this stage, however, crack openings at the notch were up to 2 mm. From a design point of view, these dimensions are excessive and so the steady-state mode-I toughness is of limited significance in this geometry.

2.4.2. Experimental observations of $(90/0/90)_s$

A single test was carried out with the laminate rotated through 90°, so the central double ply was a transverse 90° ply. The notch was cut below one of the 0° plies so that the crack would run along the 0/90 interface; this is, similar to the cracks in the four-point-bend tests, but with a single crack tip. The small offset of the crack from the central axis of the specimen results in mixed mode I/II loading. The crack initially appeared to run in the transverse ply at a depth of one or two fibres from the interface, largely following the fibre–matrix interface (Fig. 12a). Transverse ply cracks formed in the 90° ply, behind the crack tip, due to the tensile bending stresses parallel to the crack flanks. Once the crack opening was sufficient, it was clear that below the surface the crack ran in the 0° ply near the 0/90 interface, resulting in 0° fibre bridging (Fig. 12b). The delamination crack therefore behaved exactly as those in four-point-bend tests. As loading continued, the crack propagated along the specimen, but further damage evolved in the 0° ply in the crack wake, The delamination was not, therefore, a well-characterized single crack with bridging fibres, but it had a complex structure of multiple cracks and fibre bundles.

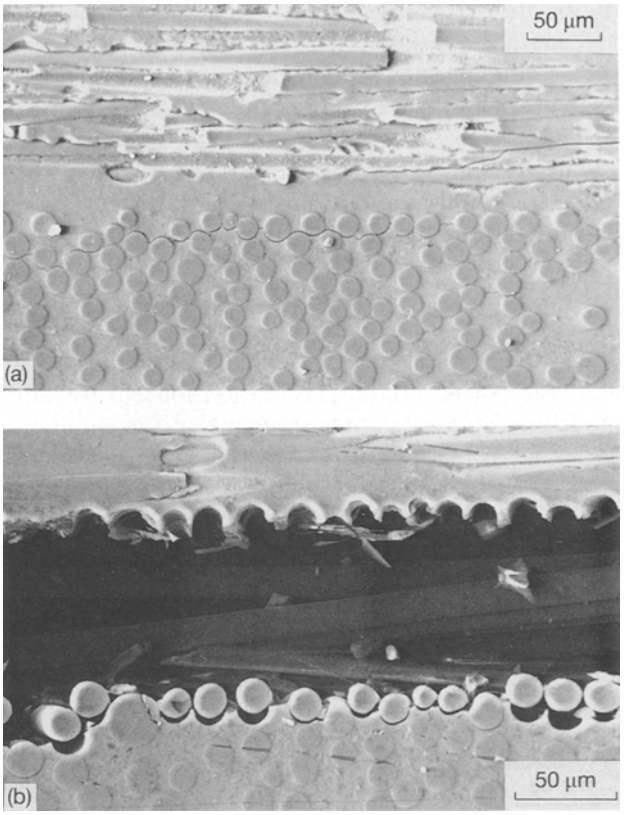

Figure 12 The development of cracks in a $(90/0/90)_s$ CAS-glass/SiC: (a) the initial crack in a 90° ply near the interface, and (b) 0° ply fibre bridging below the surface revealed at a greater crack opening.

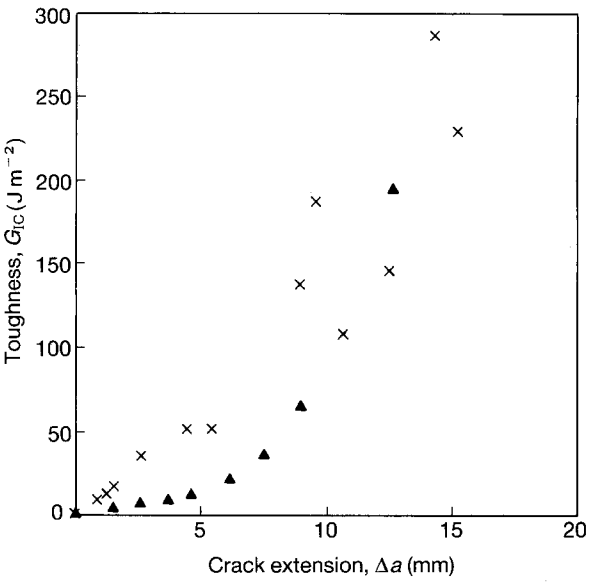

Figure 13 *R*-curves for two DCB tests on a $(0/90/0)_s$ CAS-glass/SiC: (×) specimen 1, and (▲) specimen 2.

2.4.3. Results and discussion

For the $(0/90/0)_s$ tests, the toughness G_{Ic} as a function of the crack length (the *R*-curve) was evaluated using a standard formula for this geometry [31, 32, 35, 42]:

$$G_{Ic} = \frac{12P^2a^2}{b^2h^3E} \quad (1)$$

where P is the load, a is the crack length, b and $2h$ are the specimen width and depth, and E is Young's modulus. The value for the modulus E is taken as that of the 0° plies (which dominate the bending response of the arms of the specimen), that is 137 GPa. Fig. 13 shows the *R*-curves for two specimens. Note that the toughness still increased at the limit of valid crack lengths as the specimens were too short to develop a steady-state bridging zone. The *R*-curve behaviour is marked, but (as noted above) the higher values are

only obtained with unrealistically large crack lengths and crack openings. The specimens were nominally identical but there is considerable scatter, which reflects the statistical fluctuations in fibre distribution and waviness. The data are comparable to those of Spearing and Evans [35] for tests on CAS-ceramic-matrix material, though they reached a steady-state plateau at $G_{IC} \simeq 250\,J\,m^{-2}$ since they used longer specimens.

Mixed-mode calibrations are available [31] for DCBs with offset cracks, as in the $(90/0/90)_s$ test. However, as the delamination crack produced was complex and irregular, the toughness has not been evaluated from this test. Mixed-mode data would be more readily obtained from unidirectional material with offset notches, since the bridging developed would be more uniform.

The marked mode-I R-curve stems from the closing tractions exerted by the bridging fibres. Spearing and Evans [35] modelled this R-curve by assuming that the bridging tractions result from fibre bending; that is, the exposed fibre is effectively clamped horizontally where it emerges from the crack face, and it has its ends displaced vertically as the crack opens. Our observations indicate that the fibres carry considerable tension, due to their straightness. A model for the closing traction should take this into account therefore. The magnitude of the tensile stresses in the fibres can be estimated from simple geometry. If debonding is neglected and the fibres are considered to be pinned at the crack faces, then the strain in the exposed length of fibre is $\varepsilon = (l - l_0)/l_0$ where l is the length of exposed bridging fibre, and l_0 is its original length, parallel to the crack. Substituting the angle of the fibre to the crack plane, ϕ, gives an estimate of the fibre stress

$$\sigma = E\varepsilon = E(\sec\phi - 1) \qquad (2)$$

The bridging angles were measured from a number of positions along the crack for various crack-tip positions (measuring the crack opening, u, and l_0, and noting that $\tan\phi = u/l_0$). The maximum bridging angle was found to be roughly 15°. Taking this value, which gives the highest stress, and a fibre modulus of 200 GPa, then the fibre stress would be 7 GPa. This stress may seem high compared to the quoted tensile strengths for Nicalon fibres of 1.9 GPa. However, here the length of fibre under load is of the order of 0.1–1 mm, which is much smaller than the gauge length (typically 25 mm) used to test individual fibres. Hence it is expected that the stress can be considerably above the quoted strengths, as the strength will approximately follow a Weibull distribution. In addition, debonding will occur so that a greater length of fibre can stretch to accommodate the crack opening, reducing the stress. Tensile fibre stresses above 2 GPa do not, therefore, appear unreasonable. The mode-I closing traction exerted per fibre is given by $(\sigma \sin\phi)\pi d^2/4$, where d is the fibre diameter. For a diameter of 10 μm, we therefore estimate the maximum closing force per fibre as being of the order of 40–100 mN. These calculations are very approximate but they indicate that a full model of bridging behaviour in DCB tests should take due account of the fibre tensile stresses. Such a model has been developed recently by Kaute *et al.* [43], using more detailed SEM observations of the same phenomena. This model also describes the failure of individual fibres, which is dominated by the bending stresses where the fibres emerge from the crack faces.

The mode-I observations show the geometrical configuration of fibres bridging a crack in the 0° ply. From this the mode-II behaviour could be inferred, assuming the same fibre-bridging geometry but now at zero crack opening – remote mode-II loading will introduce mode-II closing tractions (tensile in half the fibres, and compressive in the other half) as the faces try to slide past one another.

3. Conclusions

Failure of CAS-glass/SiC fibre cross-ply laminates by delamination was observed in four-point-bending and DCB geometries. *In situ* SEM facilities are powerful tools for accurately observing the growth of damage and the development of fibre bridging. The observations illustrated here are beyond the capabilities of most optical techniques, particularly the ability to observe cracking dynamically.

In four-point bending, the damage propagating from a surface notch was initially self-similar, but failure was very variable. The extent of delamination bridging varied from specimen to specimen (due to statistical variations in the material, and the influence of different notch depths on the damage pattern). Failure could be either by tensile fracture near to the notch, or by shear/compression failure occurring in the outer spans, depending on specimen dimensions and the extent of bridging. Four-point bending with surface notches therefore yields only limited qualitative information about delamination, and it is perhaps over-rated as a test of the strength of these materials. Elaborate modelling of bridged delaminations in this geometry does not appear justified.

Bending of $\pm$ 45 laminates revealed a rather different and interesting behaviour, with progressive failure through the specimen thickness leading to a large final curvature and considerable energy dissipation.

More reproducible delamination behaviour is observed in DCB specimens. A marked mode-I R-curve developed, albeit over unrealistic crack lengths and openings. The observations indicate that tensile stresses in bridging fibres are important, contrary to previous thinking, and this combined with the knowledge of the geometric disposal of bridging fibres across the crack allows accurate models to be developed. The observations also provide insight into the resistance which might be expected in mode-II configurations.

Acknowledgements

The authors wish to thank Mr. Alan Heaver for his assistance with all aspects of maintaining and operating the SEM facilities. The financial support of the U.S. Air Force Office of Scientific Research via Grant No. AFOSR-87-0307 is gratefully acknowledged.

References

1. K. M. PREWO, *Ceram. Bull.* **68** (1989) 395.
2. A. G. EVANS, and D. B. MARSHALL, *Acta Metall.* **37** (1989) 2567.
3. A. G. EVANS *J. Amer. Ceram. Soc.* **73** (1990) 187.
4. L. P. ZAWADA, L. M. BUTKUS and G. A. HARTMANN, *ibid.* **74** (1991) 2851.
5. B. HARRIS, R. G. COOKE and F. A. HABIB, Proceedings of the 5th European Conference on Composite Materials (ECCM), Bordeaux (Woodhead, Cambridge, 1992) p. 605.
6. B. HARRIS, F. A. HABIB and R. G. COOKE, *Proc. Roy. Soc. Lond. A* **437** (1992) 109.
7. B. F. SORENSON, R. TALREJA and O. T. SBAIZERO, *Proc. ECCM5*, Bordeaux (1992) p. 613.
8. D. B. MARSHALL and A. G. EVANS, *J. Amer. Ceram. Soc.* **68** (1985) 225.
9. A. W. PRYCE and P. A. SMITH, *J. Mater. Sci.* **27** (1992) 2695.
10. *Idem., Acta Metall. Mater.* **41** (1993) 1269.
11. D. S. BEYERLE, S. M. SPEARING and A. G. EVANS, *J. Am. Ceram. Soc.* **75** (12) (1992) 3321.
12. M. D. THOULESS and A. G. EVANS, *Acta Metall.* **36** (1988) 517.
13. M. D. THOULESS, O. SBAIZERO, L. S. SIGL and A. G. EVANS, *J. Am. Ceram. Soc.* **72** (1989) 525.
14. H. C. CAO, E. BISCHOFF, O. SBAIZERO, M. RUHLE and A. G. EVANS, *ibid.* **73** (1990) 1691.
15. D. ROUBY and G. NAVARRE, Proceedings of the Eleventh Riso International Symposium on Metallurgy and Materials Science (1990) 127.
16. T. P. WEIHS, O. SBAIZERO, E. Y. LUH and W. D. NIX, *J. Amer. Ceram. Soc.* **74** (1991) 535.
17. J. AVESTON, G. A. COOPER and A. KELLY, Proceedings of the National Physical Laboratory Conference on properties of Fibre Composites (IPC Technology, Guildford, 1971) 15.
18. D. B. MARSHALL, B. N. COX and A. G. EVANS, *Acta Metall.* **33** (1985) 2013.
19. B. BUDIANSKY, J. W. HUTCHINSON and A. G. EVANS, *J. Mech. Phys. Solids* **34** (1986) 167.
20. F. W. ZOK and S. M. SPEARING, *Acta Metall. Mater.* **40** (1992) 2033.
21. W. A. CURTIN, *J. Amer. Ceram. Soc.* **74** (1991) 2837.
22. G. D. QUINN and R. MORRELL, *ibid.* **74** (1991) 2037.
23. D. C. LARSEN and S. L. STUCHLY, in "Fibre reinforced ceramic composite–materials, processing and properties", (Noyes Publications, New Jersey, 1990) ch. 7.
24. K. M. PREWO, *J. Mater. Sci.* **21** (1986) 3590.
25. R. K. BORDIA, B. J. DALGLEISH, P. G. CHARALAMBIDES and A. G. EVANS, *J. Amer. Ceram. Soc.* **74** (1991) 2776.
26. O. SBAIZERO, P. G. CHARALAMBIDES and A. G. EVANS, *ibid.* **73** (1990) 1936.
27. Z. SUO, *J. Appl. Mech.* **57** (1990) 627.
28. M. Y. HE, H. C. CAO and A. G. EVANS, *Acta Metall. Mater.* **38** (1990) 839.
29. G. BAO, B. FAN and A. G. EVANS, *Mechanics of Mater.* **13** (1990) 59.
30. G. BAO, S. HO, Z. SUO and B. FAN, *Int. J. Solids Structures* **29** (1992) 1105.
31. Z. SUO, G. BAO, B. FAN and T. C. WANG, *ibid.* **28** (1991) 235.
32. Z. SUO, G. BAO and B. FAN, *J. Mech. Phys. Solids* **40** (1992) 1.
33. M. Y. HE and A. G. EVANS, *J. Comp. Tech. Res.* **14** (1992) 235.
34. G. BAO and Z. SUO, *Appl. Mech. Rev.* **45** (1992) 355.
35. S. M. SPEARING and A. G. EVANS, *Acta Metall. Mater.* **40** (1992) 2191.
36. H. R. SHERCLIFF, G. VEKINIS, M. G. ASHBY and P. W. R. BEAUMONT, Cambridge University Engineering Department Technical Report CUED/C-MATS/TR198, March (1992).
37. *Idem.* Cambridge University Engineering Department Technical Report CUED/C-MATS/TR203, September (1992).
38. G. VEKINIS, H. R. SHERCLIFF and P. W. R. BEAUMONT, *Metals and materials*, Institute of Metals, London, May (1991) 279.
39. Handbook of Materials Science, Vol. 2, edited by C. T. Lynch, (CRC Press, 1974).
40. W. J. CLEGG, K. KENDALL, N. McN. ALFORD, T. W. BUTTON and J. D. BIRCHALL, *Nature* **347** (1990) 455.
41. M. F. ASHBY K. E. EASTERLING, R. HARRYSON and S. K. MAITI, *Proc. Roy. Soc. Lond. A* **398** (1985) 261.
42. S. HASHEMI, A. J. KINLOCH and G. WILLIAMS, in "Composite materials: fatigue and fracture", Vol. 3, ASTM STP1110, edited by K. O'Brien, American Society for Testing Materials, Philadelphia (1991) p.143.
43. D. KAUTE, H. R. SHERCLIFF and M. F. ASHBY, *Acta Metall. Mater.* **41** (1993) 1959.

Received 22 October 1993
and accepted 6 January 1994